IET Electric Power Applications

Research Article

IET Journals
The Institution of Engineering and Technology

Fourier-based effective permeability for transformer iron losses computation under saturation

ISSN 1751-8660
Received on 29th April 2020
Revised 14th October 2020
Accepted on 19th October 2020
E-First on 19th January 2021
doi: 10.1049/iet-epa.2020.0315
www.ietdl.org

Wei Wang[1] ✉, *Arne Nysveen*[1], *Niklas Magnusson*[2], *Robert Nilssen*[1]

[1]*Electric Power Department, Norwegian University of Science and Technology, NO-7491 Trondheim, Norway*
[2]*SINTEF Energy Research, NO-7465 Trondheim, Norway*
✉ *E-mail: weiwan@ntnu.no*

Abstract: Computation of iron losses in transformers requires significant numerical efforts, particularly under magnetic saturation when the magnetic non-linearity needs to be considered. This study proposes a Fourier method to calculate the magnetic flux density used for the iron loss evaluation in transformers under saturation. It includes pre-processing of the non-linear material. A permeability frequency spectrum is obtained from Fourier analysis, where the fundamental part is used as a magnetisation definition and the harmonic components are used for core loss calculation. The proposed method offers a time-efficient tool to calculate core loss under various saturation levels and non-sinusoidal excitation currents. The influence of the definition of the core material on the leakage field and the stray loss calculation is studied and compared with existing methods. The proposed methods have been implemented and validated in two- and three-dimensional finite-element models with isotropic and anisotropic cores. The results yield accuracy comparable to that of a time-domain calculation. Furthermore, the influences of various effective permeability methods on the leakage field and the associated stray loss are compared and discussed.

1 Introduction

The finite-element method (FEM) is widely used to determine the magnetic field for the calculation of the iron losses in power transformers. In the linear region of ferromagnetic materials, time-harmonic representation is proved to be both efficient and accurate. However, e.g. at ferromagnetic resonance and geomagnetically induced currents when the transformer core enters its non-linear region, the employed time-domain simulation becomes very time-consuming.

For system analysis, design parameter optimisation, and inverse problem analysis where the computation effort is demanding, the frequency domain method is preferred to obtain sufficiently accurate estimations at moderate computation times. Therefore, effective permeabilities of various types [1–3] have been proposed to handle the non-linearity of the ferromagnetic cores. Energy-based methods [1, 2] are derived from the conservation of the exchange of the magnetic energy (or co-energy). DC method [2] and root mean square (RMS) method [3] and are based on the time average and the RMS of the field quantities. The choice of which existing definition of the effective permeability should be used is based on the applications [3]. In addition to the effective permeability approach, a harmonic balance method has been proposed, yielding a moderate calculation effort, but involving a reformulation of the finite-element equations in the harmonic frequency domain [4]. The material anisotropy of the core has been emphasised and treated in combination with magnetic nonlinearity [5].

When the magnetic field distribution is obtained from the finite-element analysis (FEA), the core loss can be calculated according to the existing post-processing methods, either based on loss separation (into hysteresis loss, classical eddy current loss, and excessive loss) [6] or based on curve fitting using the Steinmetz equation. For the latter, several modified types [7–11] of the Steinmetz equation have been proposed to handle non-sinusoidal excitation. The macroscopic methods [7–11] enable an efficient post-processing approach to evaluate core loss, based on the waveform of the magnetic flux density. However, since the existing effective magnetic permeability definitions [1–3] do not reproduce the flux density waveform, they cannot always provide core loss estimation accurately. Therefore, the conventional definitions of effective permeability have restricted applicability for loss evaluation, i.e. the magnetic core should be linear or slightly non-linear and the excitation should be sinusoidal.

To take both the spatial distribution and the time variation of the flux density into account, while maintaining a short computation time, we propose a method where the effective permeability is based on a Fourier series of the magnetisation curve. With the described method, the average flux density spectrum in a transformer core under saturation and non-sinusoidal excitation can be produced. For the inhomogeneous field, a modified formulation and a domain decomposition approach are introduced to improve the accuracy.

Unlike the conventional methods that only provide a single equivalent field; the proposed method preserves the full information of the magnetic field spectrum. In that way, it is possible to reduce the error of the flux density prediction considerably compared to the conventional methods. Furthermore, since the time-harmonic feature is maintained, the system size (memory requirement) and the computation effort are significantly lower compared to the harmonic balance method [4] and the time-periodic FEM [12]. The concept of degree of non-linearity (DoN) is introduced to characterise the inhomogeneity of the flux distribution, which makes domain decomposition adaptive to different core structures. This systematic approach allows an evaluation of the flux density for different core topologies under various excitations.

2 Effective permeability and flux density spectra

2.1 Model overview

A stepwise overview of the main ideas of the model is given below. Later in the paper, the key first step is explained mathematically in detail and additionally, a further accuracy improvement using domain decomposition is described, as well as a generalisation to non-sinusoidal excitation currents.

2.1.1 Fourier series definition of the magnetic permeability: Consider Fig. 1. A sinusoidal magnetic field

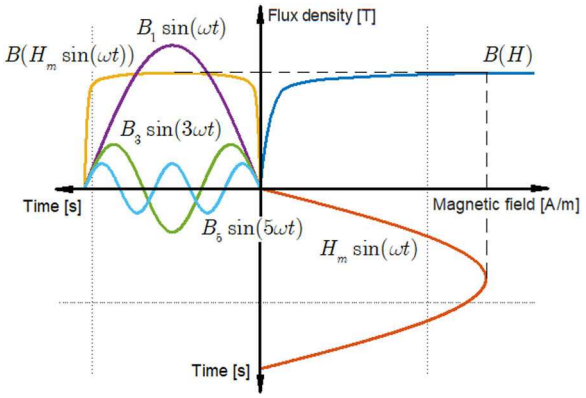

Fig. 1 *Schematic illustration of the decomposition of the magnetisation curve into a Fourier series. The fourth quadrant: a sinusoidal magnetic field strength excitation (orange); the first quadrant: the virgin B–H curve (dark blue); the second quadrant: the flux density response (yellow) and its harmonic contents (from first up to fifth order)*

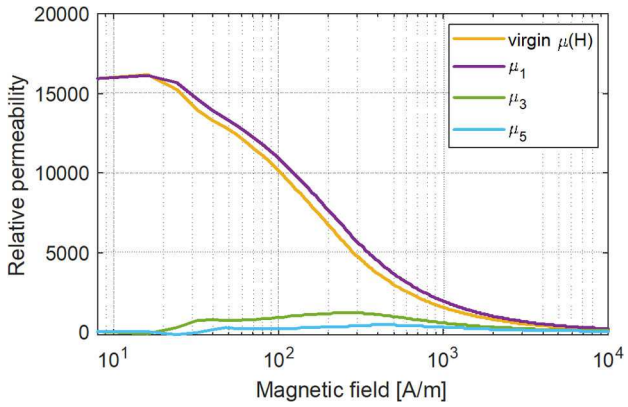

Fig. 2 *Example of effective permeability curves for individual harmonics obtained by the FM*

strength (orange) is given. When the magnetic field strength is in the saturated region of the $B(H)$ curve (dark blue), the resulting magnetic flux density (yellow) becomes non-sinusoidal. By a Fourier series definition of the magnetic flux density and thereby the magnetic permeability, the complete waveform of the magnetic flux density is preserved. The fundamental, third, and fifth harmonic components of the magnetic flux density are shown in purple, green, and light blue, respectively.

2.1.2 Finite-element implementation: A time-harmonic FEM calculation is performed to obtain the spatial distribution of the fundamental component of the magnetic flux density. In this calculation, the fundamental magnetic permeability (obtained in step 1) is used to define the effective $B(H)$ curve.

2.1.3 Retrieving the complete magnetic flux density waveform: From the spatial distribution of the fundamental component of the magnetic flux density and the pre-calculated Fourier series coefficients of the magnetic permeability, the complete waveform of the magnetic flux density is retrieved for the core (and can be used for loss calculation).

2.2 Magnetodynamic problem with the quasi-static time-harmonic representation

The governing equation of a magneto-dynamic problem is expressed by the magnetic vector potential [13]

$$\nabla \times \left(\frac{1}{\mu}\nabla \times A\right) + \sigma\frac{\partial A}{\partial t} = J_s \tag{1}$$

where μ is the magnetic permeability of the material, σ is the electric conductivity, $\boldsymbol{A}$ is the magnetic vector potential, and $\boldsymbol{J}_s$ is the current density of the external source.

For sinusoidal time variation, the complex formulation is often applied. Maxwell's equations can be formulated with quasi-static time-harmonic representation [13]

$$\nabla \times \left(\frac{1}{\mu}\nabla \times \tilde{A}\right) + \mathrm{j}\sigma\omega\tilde{A} = \tilde{J}_s \tag{2}$$

where ω is the angular frequency, and $\widetilde{\boldsymbol{A}}$ and $\widetilde{\boldsymbol{J}}_s$ are then vectors with phasor representation [13]

$$A(\mathrm{t}) = \mathscr{R}\left\{\tilde{A}\mathrm{e}^{\mathrm{j}\omega t}\right\} \tag{3}$$

$$J_s(\mathrm{t}) = \mathscr{R}\left\{\tilde{J}_s\mathrm{e}^{\mathrm{j}\omega t}\right\} \tag{4}$$

For evaluating stray loss on the tank walls or the structural parts, the surface impedance (SI) method enables a frequency domain analysis of electromagnetic fields and eddy current loss on iron surfaces. The eddy current loss in the iron tank or the structural parts subjected to a magnetic field can be calculated by [14]

$$P = \int\int_s \mathscr{R}\{Z_s\}\frac{H_\mathrm{m}^2}{2}\mathrm{d}s \tag{5}$$

where the SI Z_s is expressed as [14]

$$Z_s = \sqrt{\frac{\omega\mu}{2\sigma}}(1+j) \tag{6}$$

2.3 Defining the effective permeability using the Fourier method (FM)

For the case with magnetic saturation of the core, the magneto-dynamic problem becomes non-linear, with a non-sinusoidal magnetic flux density. To avoid the non-linearity, while at the same time preserving the complete waveform of the magnetic flux density, we introduce a Fourier series representation of the effective magnetic permeability

$$\mu_{eff,k} = \frac{\mathscr{F}_k\{B(H_\mathrm{m}\sin(\omega t))\}}{H_\mathrm{m}} \tag{7}$$

where the $B(H)$ function is the virgin non-linear magnetisation curve of the material and $\mathscr{F}_k$ is the Fourier operator giving the kth Fourier series coefficient. The numerator $B(H_\mathrm{m})$ is decomposed into Fourier series, and the denominator is the magnitude of magnetic field strength H_m. The obtained set of magnetic permeability functions are shown in Fig. 2.

The fundamental coefficient μ_1 in (7) defines the $B(H)$ curve in a FEA to obtain the spatial distribution of the flux density. The harmonic coefficients are, together with the distribution of the fundamental component, used to retrieve the complete flux density waveform in the entire core.

3 Simulations

3.1 Transformer core model

To compare the FM definition of the effective permeability (7) with an accurate (but largely time-consuming) time-domain method, a two-dimensional (2D) test case was set up, with its geometry given in Fig. 3. The simulations were performed at 50 Hz on a 60 mm long and 40 mm wide single-phase transformer core. In Fig. 4, the virgin B–H curves for the silicon steel of the core and the carbon steel of the tank are given.

In the frequency domain finite-element model, the effective B–H curve, based on the fundamental coefficient of definition (7), was implemented for the transformer core, and then in the next step, the average flux density spectrum was retrieved using the

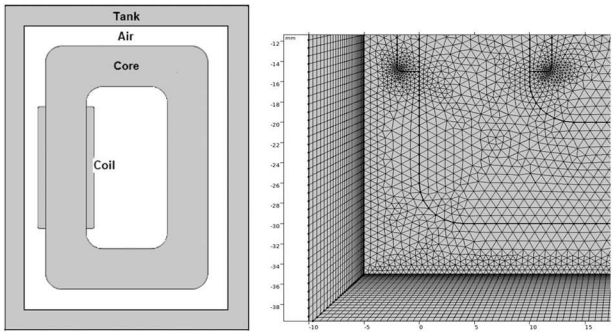

Fig. 3 *2D single-phase transformer model*
(a) Geometry, ***(b)*** Refined mesh close to the iron wall surface in the time-domain FEA

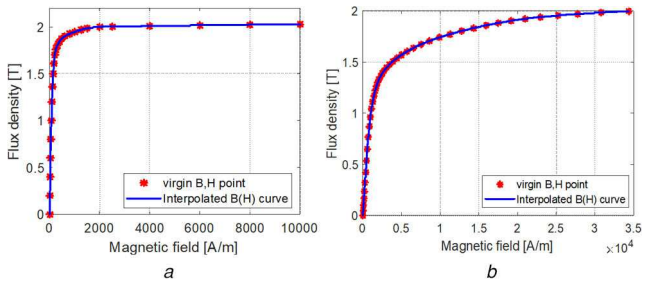

Fig. 4 *Virgin magnetisation B–H curves. The piecewise cubic interpolations are used in the curve fitting*
(a) Silicon steel of the transformer core, ***(b)*** Carbon steel of the tank

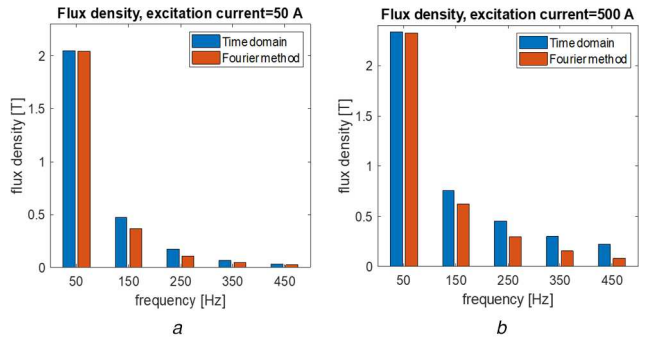

Fig. 5 *Volumetric average flux density spectra calculated the time domain method (blue) and the FM (red) under different saturation levels*
(a) Excitation current = 50 A, ***(b)*** Excitation current = 500 A

harmonic components of (7). In the time domain model, the virgin magnetisation curve was used.

3.2 Flux density spectra under sinusoidal excitation (without domain decomposition)

The average flux density spectra of the core under moderate saturation (50 A) and heavy saturation (500 A) were calculated. In Fig. 5, the results obtained by the FM are compared to the results of the corresponding time-domain simulation.

The FM shows good agreement with the time domain simulation for the fundamental component of the flux density, but underestimates the harmonic flux densities. The mismatch originates from the pre-assumption in (7) that the magnetic field H is uniformly proportional to the input excitation current, yielding a sinusoidal magnetic field $H_{\mathrm{m}}\sin(\omega t)$. However, in reality, there is a non-linear relationship between H and the current excitation, which results in a non-sinusoidal response of the magnetic field. Moreover, this dependency is not uniform in the core. The non-linearity and inhomogeneity can be considerable even under unsaturated conditions and require special handling.

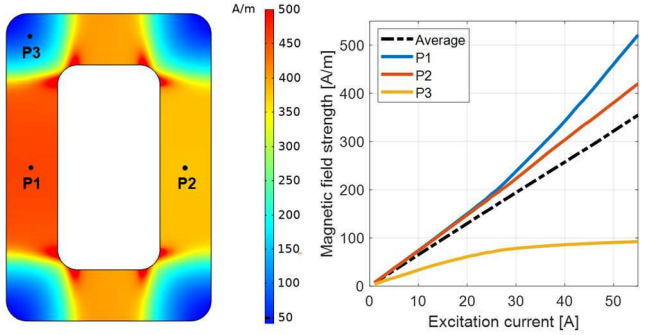

Fig. 6 *Magnetic field distribution in the transformer core. Three points are selected to demonstrate the variation of the magnetic field strength with respect to the excitation current*
(a) Magnetic field distribution, ***(b)*** Magnetic field as a function of the excitation current at points P1, P2, and P3, as well as the average magnetic field over the entire core region

3.3 Domain decomposition and a modified effective permeability

Fig. 6 shows the magnetic field distribution and the response with respect to the excitation current for three representative points of the core. The variation of the magnetic field strength at these points and the spatial average magnetic field strength over the whole area are presented in Fig. 6*b*. The average magnetic field is linear with excitation current. However, the responses at the individual points are not linear. The DoN differs significantly at different locations. In particular, the response at the corner (P3) deviates mostly from linearity. Therefore, the inherent assumption of $H(I)$ being linear in (7) could introduce an error in calculating flux density, especially when such non-linearity is strong (despite the fact that the response is linear in an average sense).

The accuracy of the flux density spectrum calculation can be improved by the introduction of domain decomposition, with the establishment of the magnetic field function $H(I)$ with respect to the input excitation current in individual subdomains.

Definition (7) must then be modified to take the non-linear relationship between the magnetic field strength and the input current into account, i.e. the magnetic field strength does not have to be sinusoidal. Instead, it is a non-linear function of the input current excitation. In the new Fourier permeability definition, the numerator maintains the same as (7), and the denominator is the fundamental component of the magnetic field. This leads to a modified effective permeability

$$\mu_{\mathrm{mf-eff},k} = \frac{\mathcal{F}_k\{B(H(I_{\mathrm{m}}\sin(\omega t)))\}}{\mathcal{F}_1\{H(I_{\mathrm{m}}\sin(\omega t))\}} \tag{8}$$

where I_{m} is the amplitude of the input current.

The number of domains that need to be applied and how to choose the boundaries between domains depend on the spatial distribution and the level of non-linearity of function $B(I)$. To assist in the division into domains, a dimensionless quantity characterising the DoN of the function $B(I)$ is suggested

$$\mathrm{DoN} = \frac{\int_0^{I_{\max}} |B(H(I)) - B((H_{\max}/I_{\max})I)|\mathrm{d}I}{\int_0^{I_{\max}} B((H_{\max}/I_{\max})I)\mathrm{d}I} \tag{9}$$

where $H_{\max}$ and $I_{\max}$ are the maximum magnetic field and the maximum input current considered. The geometric meaning of DoN is illustrated in Fig. 7, where the DoN is defined by the non-linear response $B(H(I))$ and the linear response $B(H_{\max}/I_{\max} \times I)$. The quantity DoN is a number between 0 and 1, where DoN = 0 corresponds to a linear relationship between H and I and DoN = 1 corresponds to a step function.

The DoN calculated by (9) for the transformer core is illustrated in Fig. 8*a*. By means of DoN, the boundaries of the domain

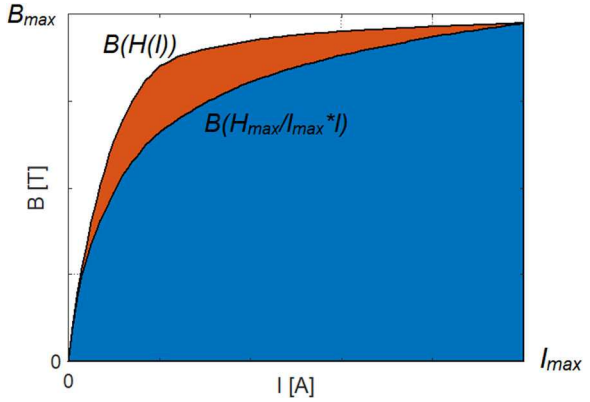

Fig. 7 *Illustration of DoN. DoN is defined as the ratio of the red area* $B(H(I)) - B(H_{max}/I_{max} \times I)$ *to the blue area* $B(H_{max}/I_{max} \times I)$

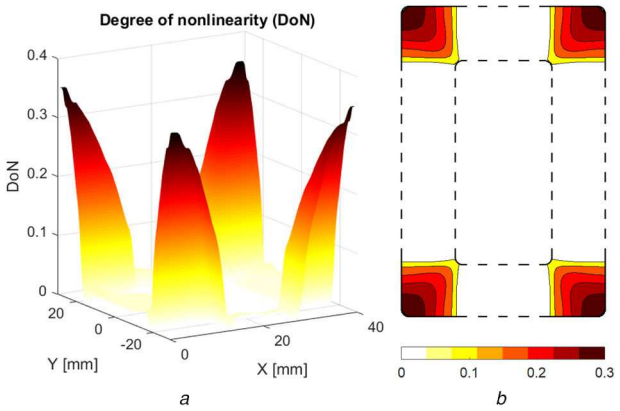

Fig. 8 *DoN calculated by definition (9) in the region of the transformer core*

(a) Plot of DoN, ***(b)*** Contour of the DoN is used to determine the domain boundaries

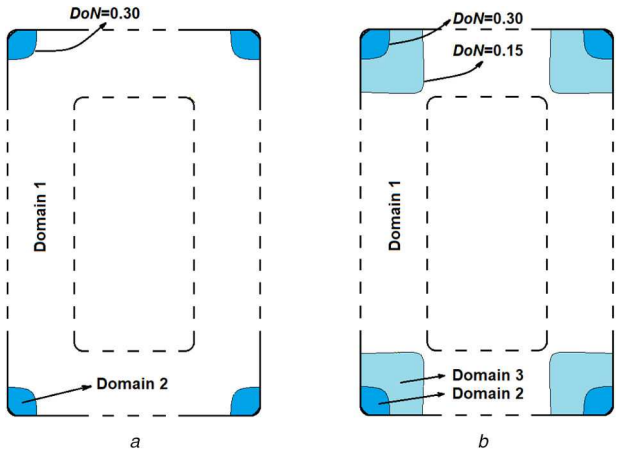

Fig. 9 *Illustration of domain decomposition by different levels of DoN contours*

(a) Domain division by a single DoN contour, DoN = 0.30, ***(b)*** Domain division by two DoN contour lines, DoN = 0.15 and 0.30

division are simply the projections of different DoN levels on the domain, i.e. the contour of the DoN (Fig. 8*b*).

3.4 Flux density spectra under sinusoidal excitation (with domain decomposition)

Generally, regions with small differences in DoN can be treated together. For practical reasons, coarse domain decomposition is preferred. Two simple schemes were adopted to demonstrate the domain division by DoN: a single contour line with DoN = 0.30; two contour lines with DoN = 0.15 and 0.30. The resulting domain divisions are shown in Fig. 9.

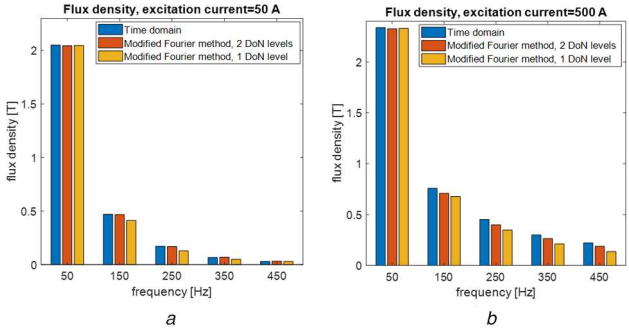

Fig. 10 *Volumetric average flux density spectra calculated with different methods (blue: time-domain method; red: modified FM) under different saturation levels*

(a) Excitation current = 50 A, ***(b)*** Excitation current = 500 A

Table 1 Error comparison by different FMs

Excitation current, A	FM without domain decomposition, %	FM with 1 level of DoN, %	FM with 2 levels of DoN, %
50	6.1	3.6	0.4
500	12.3	7.7	3.8

The two domain decomposition schemes were adapted to the transformer core and the modified effective permeability definition (8) was applied to the individual domain. The calculated flux density spectra were compared to the time domain simulation result (Fig. 10).

To quantify and compare the accuracy of the average flux density calculation using different methods, a spectrum-based error estimation (10) is introduced to characterise the difference relative to the time-domain result and the comparison is given in Table 1

$$\varepsilon_B = \frac{\sqrt{\sum_{i=1}^{n}(B_{\mathrm{TD},i} - B_{\mathrm{FD},i})^2}}{B_{\mathrm{TD},1}} \tag{10}$$

where $B_{\mathrm{FD},i}$ is the calculated amplitude of the average flux density at the harmonic order i; $B_{\mathrm{TD},i}$ is the amplitude of the average flux density at the harmonic order i, calculated from a time-domain simulation.

As shown in Fig. 10 as well as in Table 1, the calculated flux density spectra (red and yellow columns) show a significantly better agreement (compared to without the modifications) with the results from the time-domain simulation (blue columns). Moreover, the decomposition of the domain into more regions improves the accuracy of the flux density calculation. Under moderate saturation (50 A), a decomposition with a single DoN is sufficient (ε_B = 3.6%), whereas, under heavy saturation (highly non-linear), more domains are required with multiple DoN contours.

The non-linearity and inhomogeneity also depend on the configuration and the material properties of the magnetic core. In the case of a configuration with a more uniform flux distribution such as a toroid core, definition (7) could offer sufficient accuracy without domain decomposition.

3.5 Validation in 3D case

The FM as well as the domain decomposition approach are further validated in 3D models. An isotropic material, i.e. non-grain-oriented (NGO) material (the magnetic properties are identical to Fig. 4*a*) is defined for the core. Apart from isotropic materials, grain-oriented (GO) electrical steel is widely used in energy-efficient transformers and large, high-performance generators. As a comparison, a 3D model with the anisotropic core is established. The permeability tensor μ is defined as

$$\mu = \begin{bmatrix} \mu_r & & \\ & \mu_t & \\ & & \mu_n \end{bmatrix} \quad (11)$$

where μ_r is the permeability in the rolling direction, defined by Fig. 4*a*; μ_t is the permeability in the direction that is transverse to the rolling direction (in the same lamination plane); to be simple, the quantity of μ_t is assumed to be $0.02\mu_r$. μ_n is the equivalent permeability in the direction normal to the lamination plane. Owing to the lamination structure, μ_n is small (the value is determined by the stacking factor of the lamination) and 30 is assumed in the calculation [15]. The off-diagonal elements are assumed to be zero. The excitation currents are 100 A for both simulations. The flux density distributions from time-domain simulations are shown in Fig. 11.

As shown in Fig. 11, the flux density distribution is nearly homogeneous in the GO core, whereas the flux density is strongly inhomogeneous in the isotropic core. FM-based permeability is applied to both models, where the calculated spectra are compared to the corresponding time-domain simulation result (Fig. 12) and the errors are presented in Table 2. Owing to the homogeneity of the flux distribution in the anisotropic core, the FM (7) gives an accurate estimation (Fig. 12*b*, $\varepsilon_B = 0.4\%$) of the flux density spectrum without domain decomposition. For the isotropic core, the FM (7) gives a moderate accurate result (Fig. 12*a*, $\varepsilon_B = 3.3\%$). With a single domain decomposition, the accuracy is improved (Fig. 12*a*, $\varepsilon_B = 1.6\%$).

3D models are always preferred for calculating core losses, not only because the magnetic core has 3D structure, but also from the perspective of the flux homogeneity. The actual flux distribution can vary significantly in space, both globally and locally. It is shown in Fig. 11 that the flux density varies much more in the corners and joints than in the limbs/yokes for the isotropic material. The GO material can significantly improve the homogeneity. Studies also show that the flux around holes [16] and along the edges [17] can be inhomogeneous. In addition, the leakage flux penetrating the core lamination makes the superimposed flux saturate the surface and edges of the steel in the proximity of the winding terminals [18]. The above-mentioned scenarios involve the flux distribution with 3D nature, and require special handling of inhomogeneous effects.

3.6 Flux density spectra under non-sinusoidal excitation

Definition (8) can be further generalised to non-sinusoidal excitation currents, occurring e.g. at voltage over-excitation. The current in (8) is then defined as a general function $I(t)$. Like in (7), the fundamental component of the resultant magnetic field is used as the denominator in the permeability definition. Hence, the generalised effective permeability becomes

$$\mu_{\mathrm{gf-eff},k} = \frac{\mathcal{F}_k\{B(H(I(t)))\}}{\mathcal{F}_1\{H(I(t))\}} \quad (12)$$

To validate the generalised Fourier effective permeability definition under non-sinusoidal excitation, two test cases with different input currents were set up

- Case 1: $I_1 = 50\sin(100\pi t) + 10\sin(300\pi t)$ [A]
- Case 2: $I_2 = 50\sin(100\pi t) - 10\sin(300\pi t)$ [A]

The cases have the same fundamental input current, but the third harmonics are of opposite phases. Again, the domain decomposition scheme was applied.

The calculated flux density spectra (using the FM) show a good agreement with the time domain simulation results, see Fig. 13. In Fig. 14, the corresponding time-domain waveforms are shown (for the FM using up to the ninth harmonic), confirming the good agreement.

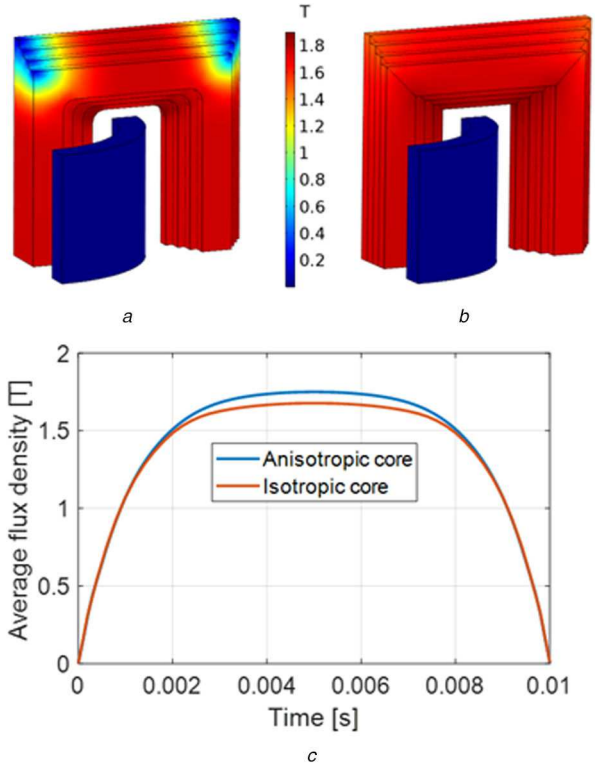

Fig. 11 *Flux density distribution in the transformer core (a quarter model) from a time-domain simulation*
(a) Isotropic magnetic core, ***(b)*** Anisotropic (GO) magnetic core, ***(c)*** Average flux density variation over half period

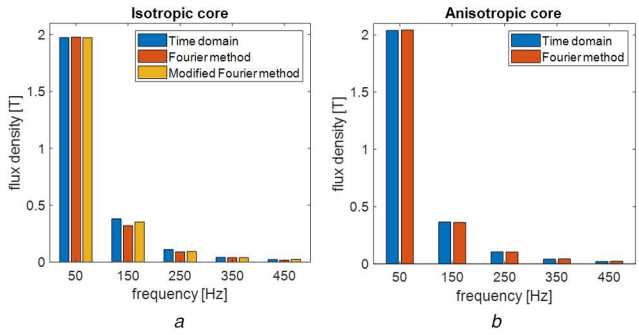

Fig. 12 *Volumetric average flux density spectra calculated for the magnetic core with different materials*
(a) Isotropic (NGO) magnetic core, ***(b)*** Anisotropic (GO) magnetic core

Table 2 Error for different core types

Excitation current, A	FM, NGO steel, %	Modified-FM, NGO steel, %	FM, GO steel, %
100	3.3	1.6	0.4

3.7 Core loss

Using the effective permeability definition (7), (8), and (12), the waveform of the flux density can be retrieved. When calculating flux density waveform, only the magnetisation curve is considered and the hysteresis effect on the resultant flux density is neglected. In the formulation of the modified Steimeltz equation [7] and the generalised Steimeltz equation [11], the flux density and its time-derivative are the only required inputs (other coefficients are obtained by material characterisation). Then, using any of the existing macroscopic methods [7–11], the core loss can be calculated with sufficient accuracy. Since both pre-processing and post-processing treatments are offline, the advantage of computation efficiency of the time-harmonic method is maintained. Detailed implementation of the macroscopic methods and calculation of core loss is then trivial.

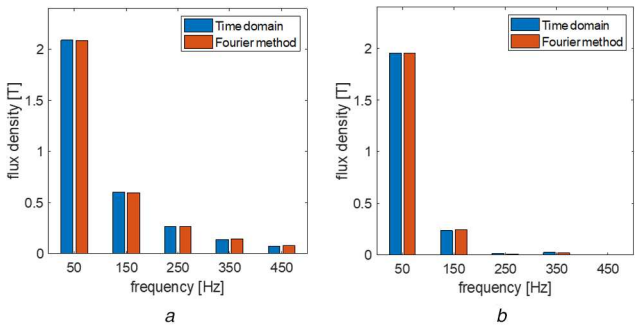

Fig. 13 *Average flux density spectra calculated with the time domain method (blue) and the generalised FM (red)*
(a) Case 1, ***(b)*** Case 2

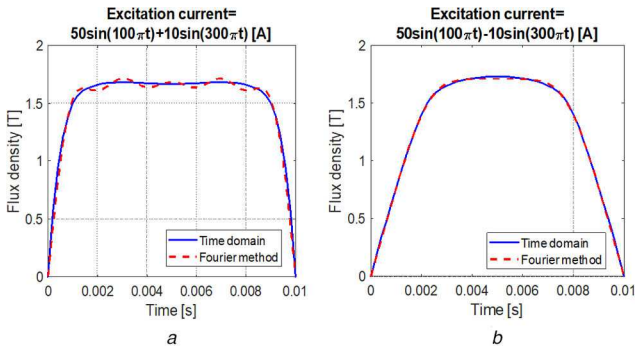

Fig. 14 *Average time-domain waveforms calculated with the time domain method (blue) and the generalised FM (red)*
(a) Case 1, ***(b)*** Case 2

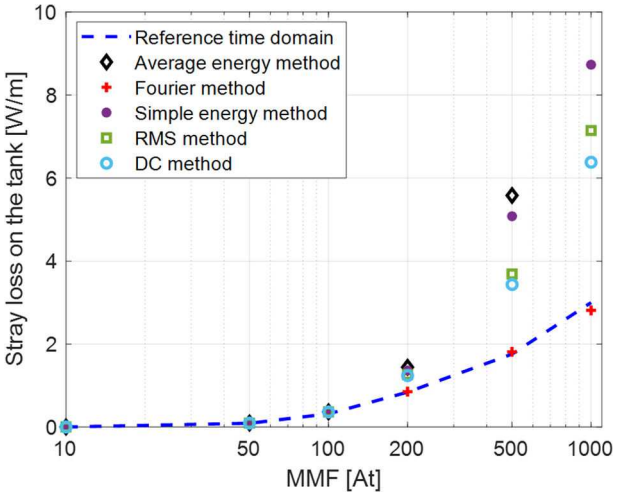

Fig. 15 *Stray loss in the transformer tank wall calculated by various effective permeability methods under different saturation levels*

3.8 Stray loss

To evaluate the influence of the permeability definitions of the core material on stray loss calculation, a single-phase transformer FEM model (Fig. 3) was set-up and the time-harmonic simulations were performed with the magnetomotive force (MMF) varying from 10 to 1000 A·t. The MMF ranges from the linear region to the heavily saturated region of the non-linear material. We implemented definition (7) as well as the methods proposed [1–3] in the transformer core, whereas in the time-domain model, the virgin magnetisation curves (Fig. 4) were used. The eddy current loss was calculated by the SI method (5). The results are compared with the results obtained by the time-domain method (accurate but largely time-consuming), see Fig. 15.

For a moderate excitation current (MMF <100 A·t), the magnetic core is in the linear or slightly non-linear region. The different definitions of the effective permeability yield result practically equal to those calculated with the time domain method (maximum deviation <6%), and hence, are good estimations of the stray loss. However, when the excitation current is more significant (MMF >100 A·t), the core is in the heavily saturated region, and then the conventional methods largely overestimate the losses, and thereby they are not suitable for stray loss evaluation. In contrast, the FM (7) gives a good estimation of the stray loss over the whole range.

Furthermore, in [19], a waveform correction factor is proposed in combination with the effective permeability, which enables an evaluation of the stray loss for non-sinusoidal current excitation under saturation.

4 Conclusions

With the described FMs, a time-harmonic analysis to calculate the average flux density spectrum in a transformer core under saturation yields an accuracy comparable to that of a time-domain calculation. In a magnetic core with a homogeneous distributed flux such as the one made of GO steel, the original formulation (without domain decomposition) gives sufficiently accurate results. In the case of inhomogeneously distributed flux under heavy saturation, the modified formulation with domain decomposition significantly improves the accuracy. DoN is introduced to assist domain decomposition. Under a moderate saturation, a single domain decomposition is sufficient, whereas, under heavy saturation (highly non-linear), two and more domain divisions are needed.

Combined with the existing macroscopic loss calculation methods, the FM offers a time-efficient tool to accurately calculate core loss under various saturation levels and non-sinusoidal excitations. Moreover, the FM yields significantly higher accuracy in stray loss calculation under heavy saturation than energy-based methods.

5 Acknowledgments

This work was performed as a part of the project 'Thermal Modelling of Transformers' (project number: 255178) funded by the Research Council of Norway, Statnett, Hafslund, and Lyse Nett.

6 References

[1] Hedia, H., Remacle, J.F., Dular, P., *et al.*: 'A sinusoidal magnetic field computation in nonlinear materials', *IEEE Trans. Magn.*, 1995, **31**, (6), pp. 3527–3529
[2] Labridis, D., Dokopoulos, P.: 'Finite element computation of eddy current losses in nonlinear ferromagnetic sheaths of three-phase power cables', *IEEE Trans. Power Deliv.*, 1992, **7**, (3), pp. 1060–1067
[3] Paoli, G., Biro, O., Buchgraber, G.: 'Complex representation in nonlinear time harmonic eddy current problems', *IEEE Trans. Magn.*, 1998, **34**, (5), pp. 2625–2628
[4] Yamada, S., Bessho, K.: 'Harmonic field calculation by the combination of finite element analysis and harmonic balance method', *IEEE Trans. Magn.*, 1988, **24**, (6), pp. 2588–2590
[5] Steinmetz, T., Cranganu-Cretu, B., Smajic, J., *et al.*: 'Investigations of no-load and load losses in amorphous core dry-type transformers'. The XIX Int. Conf. on Electrical Machines-ICEM, Rome, Italy, 2010, p. 11615029
[6] Barbisio, E., Fiorillo, F., Ragusa, C.: 'Predicting loss in magnetic steels under arbitrary induction waveform and with minor hysteresis loop', *IEEE Trans. Magn.*, 2004, **40**, (4), pp. 1810–1819
[7] Reinert, J., Brockmeyer, A., Doncker, R.W.: 'Calculation of losses in ferro- and ferrimagnetic materials based on the modified Steinmetz equation'. Proc. 34th Annual Meeting of the IEEE Industry Applications Society, vol. 3, Phoenix, USA, 1999, pp. 2087–2092
[8] Yue, S., Li, Y., Yang, Q., *et al.*: 'Comparative analysis of core loss calculation methods for magnetic materials under nonsinusoidal excitations', *IEEE Trans. Magn.*, 2018, **54**, p. 6300605
[9] Alatawneh, N., Rahman, T., Hussain, S., *et al.*: 'Accuracy of time domain extension formulae of core losses in non-oriented electrical steel laminations under non-sinusoidal excitation', *Electr. Power Appl. IET*, 2017, **11**, (6), pp. 1131–1139
[10] Agheb, E, Hoidalen, H.K.: 'Modification of empirical core loss calculation methods including flux distribution', *IET Electr. Power Appl.*, 2013, **7**, pp. 381–390
[11] Jieli, L., Abdallah, T., Sullivan, C.R.: 'Improved calculation of core loss with nonsinusoidal waveforms'. IEEE Industry Applications Society Annual Meeting, Chicago, USA, October 2001, pp. 2203–2210
[12] Takahashi, Y., Iwashita, T., Nakashima, H., *et al.*: 'Parallel time-periodic finite-element method for steady-state analysis of rotating machines', *IEEE Trans. Magn.*, 2012, **48**, (2), pp. 1019–1022
[13] Harrington, R.F.: '*Time-harmonic electromagnetic fields*' (Wiley-IEEE Press, New York, USA, 2001, 2nd edn.)

[14] Yuferev, S, Ida, N.: '*Surface impedance boundary conditions - a comprehensive approach*' (CRC Press, Boca Raton, 2009)
[15] Wang, W., Nysveen, A., Magnusson, N.: 'Eddy current loss in grain-oriented steel laminations due to normal leakage flux'. Presented at IEEE Conf. on Electromagnetic Field Computation (CEFC), Pisa, Italy, November 2020
[16] Gunes, T., Derebasi, N., Erdonmez, C.: 'Localized flux density distribution around a hole in non-oriented electrical steels', *IEEE Trans. Magn.*, 2015, **51**, (1), pp. 1–4
[17] Moses, A.J., Derebasi, N., Loisos, G.*, et al.*: 'Aspects of the cut-edge effect stress on the power loss and flux density distribution in electrical steel sheets', *J. Magn. Magn. Mater.*, 2000, **215–216**, pp. 690–692
[18] Wang, W., Nysveen, A., Magnusson, N.: 'Apparatus for loss measurements under multidirectional and dc-bias flux in electrical steel laminations', *Rev. Sci. Instrum.*, 2020, **91**, p. 084705
[19] Wang, W., Nysveen, A., Magnusson, N.*, et al.*: 'Computation of transformer iron losses under saturation using the Fourier method part 2: stray loss'. Int. Conf. on the Computation of Electromagnetic Fields, Paris, France, 2019, p. 1902008